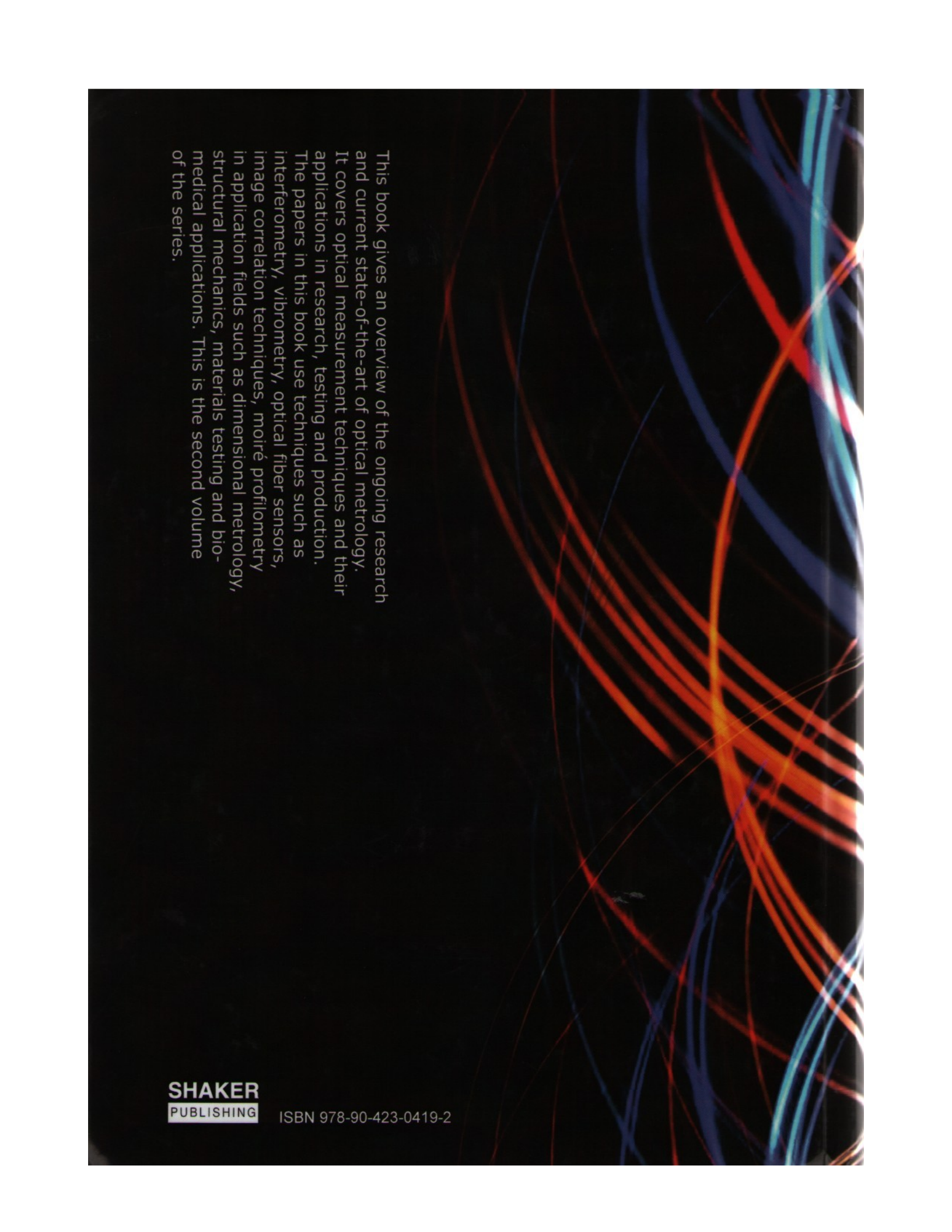


Optical Measurement Techniques
for Systems & Structures²

EDITORS
Joris Dirckx | Jan Buytaert



This book gives an overview of the ongoing research and current state-of-the-art of optical metrology. It covers optical measurement techniques and their applications in research, testing and production. The papers in this book use techniques such as interferometry, vibrometry, optical fiber sensors, image correlation techniques, moiré profilometry in application fields such as dimensional metrology, structural mechanics, materials testing and bio-medical applications. This is the second volume of the series.

SHAKER
PUBLISHING

ISBN 978-90-423-0419-2

Curvelet Transform Method for Phase-Map Denoising

Nivia Escalante^a, Jesús Villa^b, Ismael de la Rosa^c,
Osvaldo Gutiérrez^d and Ramón Rodríguez-Vera^e

Abstract

A Curvelet transform method for phase-map denoising is presented. In the problem of phase-map denoising there exist a tradeoff between the removed noise and the blurring of the image. Phase unwrapping is often required to construct a continuous phase-map from a wrapped one in optical interferometry, Interferometric Synthetic Aperture Radar, and magnetic resonance imaging; however, with the presence of noise this procedure can be difficult to realize and a previous filtering is required. The Curvelet transform has been developed as an alternative to wavelet transform in which frame elements are indexed by scale, location, and orientation parameters. The main advantage of the proposed method using the Curvelet transform is that previous estimation of the phase-map orientation information is not required, as is the case of recently reported directional filtering techniques. The presented technique, which is still in development, presents good expectations of its performance against noise with a reasonable computational effort.

Contact information

^a aivineg_2682@yahoo.com, jvillah@yahoo.com,

ismaelrv@yahoo.com, osvaldo_gtz_mt@yahoo.com

Laboratorio de Procesamiento Digital de Señales, Unidad Académica de Ingeniería Eléctrica, Universidad Autónoma de Zacatecas, Av. Ramón López Velarde #801, C.P. 98000, Zacatecas, México.

^b rarove@cio.mx

Centro de Investigaciones en Óptica, A. C., Loma del Bosque 115, Col. Lomas del Campestre C.P. 37150, Apdo.P.1-948, León, Guanajuato, México.

Acknowledgements

The authors would like to gratefully acknowledge the material support of Ergon, KU Leuven's

Introduction

Optical methods are widely used for nondestructive testing and metrology. Most experimental data obtained using full field optical metrology are encoded as a wave front (phase) which modulates the fringes of an interferometric image; the fringe patterns contain the physical information to be determined. The goal of fringe analysis is to estimate the modulating two-dimensional phase of these fringe patterns [1].

The phase unwrapping problem is an important step in fringe analysis; is a technique used on wrapped phase images to remove the 2π discontinuities embedded within the phase-map. It detects a 2π phase jump and adds or subtracts an integer offset of 2π to successive pixels following that jump is based on a threshold mechanism, thus, retrieving the contiguous form of the phase-map. Recovering the original phase value is a big challenge [2]. This information is important for a variety of applications, such as terrain elevation estimation synthetic aperture radar, field mapping in magnetic resonance imaging, wavefront distortion measurement in adaptive optics, etc.

In the case of phase-maps and interferograms linear filtering techniques do not provide satisfactory results. Linear filters have several undesirable limitations or deficiencies in some applications. These include blurring of edges while smoothing noise, sensitivity to noise while detecting edges, poor smoothing, loss of detail, very noise sensitivity [3], etc.

Some denoising techniques have been developed to improve the phase unwrapping [4, 5], for instance, the comparative analysis of some methods by Kemao *et al.* [6]. Another effective technique for filtering wrapped phase maps has been pointed out by Tang *et al.* [7] who use sine/cosine filtering with windows along tangent directions of isophase contours of ESPI (Electronic Speckle pattern interferometry) phase maps. More recently, the same author proposed the Oriented-Couple Partial Differential Equations [7] for denoising wrapped phase patterns. In both cases [4, 5] the key idea is the filtering along isophase lines (i.e. along the orthogonal direction of phase gradient). This strategy has two advantages: noise can be easily removed because phase information and noise are conveniently separated in the frequency domain, and the discontinuities of the wrapped phase map are preserved. Villa *et al.* [9] derived a regularized quadratic-cost function that uses complex-valued Markov random fields (CMRFs) which includes fringe orientation information of the filtering direction along isophase lines.

However, a drawback of all mentioned techniques is that they require the previous estimation of the so-called fringe orientation which, as it uses the computation of the image gradient, could be an inaccurate procedure in the presence of noise and low-modulation of fringes. A typical characteristic of the resulting filtered phase image is the presence of structures due to the changes of the orientation angles, which is a drawback too [8].

The importance of multiscale descriptions of images has been recognized from the early days of computer vision. Multiresolution analysis has been successfully used in image processing specially with image segmentation; wavelet-based features have been used in various applications

including image compression, denoising and classification. The uses of wavelet transform is mainly due to its good performance in representation of piecewise smooth functions in one dimension. Unfortunately this ability is lost when it is applied to two dimensions. When the wavelet transform is applied in 2-D, frequently uses separate wavelet basis which are obtained by applying 1-D wavelet transforms separately in each dimension, so it lacks of directional information, which is a substantial aspect for describing image singularities [10]. The Curvelet transform is a new extension of wavelet transform which aims to deal with an interesting phenomena occurring along curved edges in 2-D images [11]. It is a high-dimensional generalization of the wavelet transform designed to represent images at different scales and different orientations (angles). It is viewed as a multiscale pyramid with frame elements indexed by location, scale, and orientation parameters with needle-shaped elements at fine scales. Curvelets have time-frequency localization properties of wavelets but also shows a very high degree of directionality and anisotropy, and its singularities can be well approximated with very few coefficients. The main advantage of the proposed method using the Curvelet transform is that prior knowledge or estimation of the phase-map orientation information is not required, as is the case with the recently reported directional filtering techniques. We propose a technique where the most significant coefficients which are used to model the fringes.

The Curvelet transform for denoising phase-maps

Wavelet and other frequency transforms are widely used for denoising, but they suffer from shift and rotation sensitivity, as well as they are poor in directionality. The curvelet transform, like the wavelet transform, is a multiscale transform with frame elements indexed by scale, angle and location parameters. Unlike the wavelet transform, it has directional parameters and the curvelet pyramid contains elements with a very high degree of directionality. In addition, the curvelet transform is based on a certain anisotropic scaling principle which is quite different from the isotropic scaling of wavelets. Curvelets have useful geometric features that set them apart from wavelets and the likes. Curvelet transform is more suitable for detection of directionality and provides an optimal representation of objects which display curves.

Filtering wrapped phase-maps

In wrapped phase-maps there is a lot of noise which can be caused by the system temperature, overlays and inaccurate matching, etc. The filtering of the wrapped phase has great influence in the phase unwrapping but traditional filters are not adequate for it [12]. A wrapped phase map is defined as $\varphi_w(x, y)$, and can be equivalently represented by its sine and cosine terms [13]:

$$C(x, y) = \cos[\varphi_w(x, y)], \quad S(x, y) = \sin[\varphi_w(x, y)] \quad (1.1)$$

The equivalence is based on the fact that the wrapped phase can be uniquely recovered as:

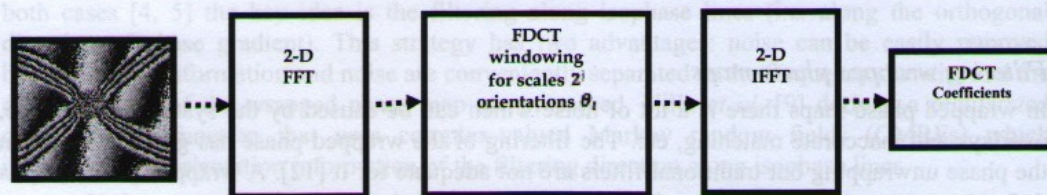
$$\varphi_w(x, y) = \arctan[S(x, y) / C(x, y)]. \quad (1.2)$$

where $\varphi_w(x, y) = \arctan(\cdot, \cdot)$ is the four-quadrant inverse tangent function. Therefore, filtering C and S , which are continuous functions, is equivalent to filter $\varphi_w(x, y)$.

Curvelet transform method for phase-map denoising

New transforms may be very significant for practical concerns. For instance, the potential for sparsity of wavelet expansions paved the way to very successful applications in areas such as signal/image denoising, feature extraction [13], etc. The curvelet transform is a particular type of transformation that can be applied to images for extracting edges and discontinuities in the image. It is derived from the wavelet transform. Curvelet transform is a multiscale pyramid with many directions, positions at each length, and scales. It is designed to represent edges and other singularities along curves much more efficiently than traditional wavelet transforms. In the curvelet transform the width and length are related by the relation $\text{width} \approx \text{length}$ that is known as parabolic or anisotropic scaling [14]. The literal meaning of curvelet is “brush strokes”. The Curvelet transform is a combination of sub-band decomposition, smooth partitioning, renormalization and Ridgelet analysis [14]. Curvelets are based on multiscale ridgelets combined with a spatial bandpass filtering operation to isolate different scales [15], [16]. Curvelets occur at all scales, locations and orientations. However, while ridgelets all have global length and variable width [17], curvelets in addition to a variable width have a variable length and so a variable anisotropy. An important ingredient of the curvelet transform is to restore sparsity by reducing redundancy across scales. In detail, one introduces interscale orthogonality by means of sub-band filtering [18]. Curvelets obey a parabolic scaling relation which says that at scale 2^{-j} , each element has an envelope which is aligned along a “ridge” of length $2^{-j/2}$ and width 2^{-j} [11].

The curvelet transform provides a near-optimal sparse representation for images having discontinuities along C^2 (twice differentiable) curves. The general steps are shown in Figure 1, after computing the two-dimensional (2-D) discrete Fourier transform (DFT) of the image using the fast Fourier transform (FFT), curvelet frequency windows at different scales and angles are applied. By computing the 2-D inverse DFT (IDFT) of each windowed output, one obtains the curvelet coefficients. The image can be recovered without error from the curvelet coefficients by inverting each involved step [18,19]. The computational complexity of the FDCT is only $O(N^2 \times \log N)$ for an $N \times N$ image [19].



Input
image

Figure 1: The data flow in the forward of FDCT

The overall of number of computations increases because the 2-D DFT is computed in each channel of the filter bank. This is J times more when compared to the original FDCT algorithm. However, the overall computational complexity remains the same as $O(N^2 \times \log N)$ for an $N \times N$ image.

The fast curvelet transform replaces the polar tiling of the Fourier domain by a recto-polar tiling, illustrated in Figure 2. The directions α are uniformly discretized so that the slopes of the wedges containing the support of the curvelets are uniformly distributed in each of the north, south, west, and east Fourier quadrants. A curvelet is a function $c(x)$ having vanishing moments along the horizontal direction like a wavelet [20]. Each wedge is the support of the two-dimensional DFT $\hat{c}_j^\alpha[k_1, k_2]$ of discrete curvelet $c_j^\alpha[n_1, n_2]$.

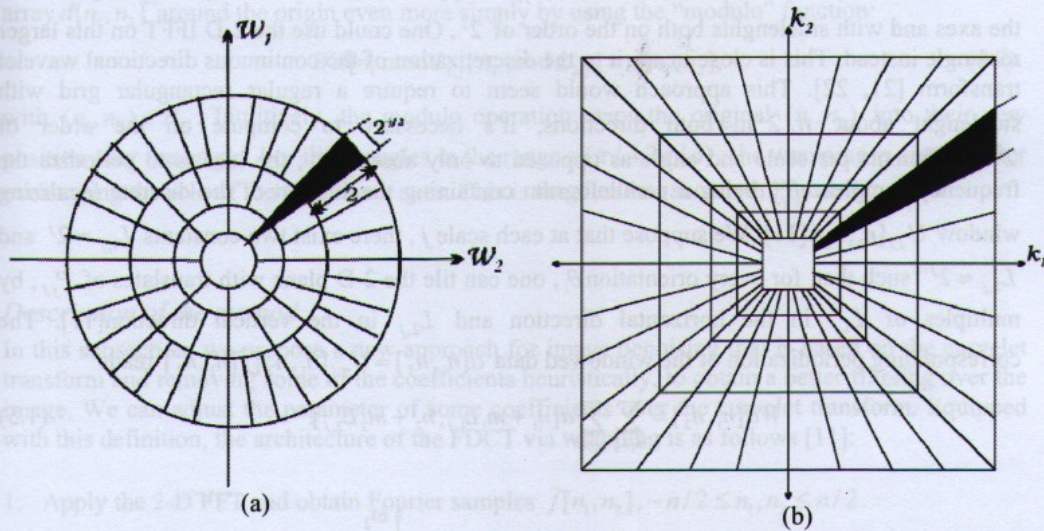


Figure 2: (a) Curvelet frequency plane tiling. The dark area is a wedge obtained as the product of a radial window and an angular window. (b) Discretized curvelet frequency tiling. The radial and angular windows define trapezoidal wedges as shown in dark.

Coronae and rotations, as in the continuous-time definition, are not especially adapted to Cartesian arrays, so it is convenient to replace these concepts by Cartesian equivalents, “Cartesian coronae” based on concentric squares (instead of circles) and shears. The digital coronae of the “wrapping” suggests Cartesian curvelets of the form $\tilde{\varphi}_{j,l,k}(x) = 2^{3j/4} \tilde{\varphi}_j(S_\theta^T(x - S_\theta^{-T}b))$ where S_θ is shear matrix; is used to maintain the symmetry around the origin and rotation by $\pm \pi/2$, b takes on the discrete values $b \cong (k_1 \cdot 2^{-j}, k_2 \cdot 2^{-j/2})$, taking on values on a rectangular grid the simpler choice of spatial grid to translate curvelets at each scale and angle and [11].

$$c(j, l, k) = \int \hat{f}(w) \tilde{U}_j(S_\theta^{-1}w) e^{i\langle b, w \rangle} dw. \quad (1.3)$$

The equation (1.3) is for b when $\theta \in (-\pi/4, \pi/4)$ or $\theta \in (-3\pi/4, 5\pi/4)$; otherwise the roles of $L_{1,j}$ and $L_{2,j}$ have to be exchanged. The difficulty behind this approach is that, in the frequency plane, the window $U_{j,l}[n_1, n_2]$ implies a concentric tiling whose geometry is pictured in Figure 2(b) and

does not fit in a rectangle of size $\approx 2^j \times 2^{j/2}$, aligned with the axes, in which the 2-D inverse fast Fourier transform (IFFT) could be applied to compute the Equation (1.3). After discretization, the integral over w becomes a sum over n_1, n_2 which would extend beyond the bounds allowed by the 2-D IFFT. We need to respect the rectangle sizes; we recall that $U_{j,l}$ is supported in the parallelepipedal region.

$$P_{j,l} = S_\theta P_j. \quad (1.4)$$

For most values of the angular variable θ , $P_{j,l}$ is supported inside a rectangle $R_{j,l}$ aligned with the axes and with sidelengths both on the order of 2^j . One could use the 2-D IFFT on this larger rectangle instead. This is close in spirit to the discretization of the continuous directional wavelet transform [21, 22]. This approach would seem to require a regular rectangular grid with sidelength about $n/2^j$ in both directions, it's necessary to compute on the order of 2^{2j} coefficients per scale and angle as opposed to only about $2^{3j/2}$; the idea is to periodize the frequency samples. $P_{j,l}$ being a parallelogram containing the support of the discrete localizing window $U_{j,l}[n_1, n_2]$ [11]. We suppose that at each scale j , there exist two constants $L_{1,j} \approx 2^j$ and $L_{2,j} \approx 2^{j/2}$ such that, for every orientation θ , one can tile the 2-D plane with translates of $P_{j,l}$, by multiples of $L_{1,j}$ in the horizontal direction and $L_{2,j}$ in the vertical direction [11]. The corresponding periodization of the windowed data $d[n_1, n_2] = U_{j,l}[n_1, n_2] \hat{f}[n_1, n_2]$ reads

$$Wd[n_1, n_2] = \sum_{m_1 \in \mathbb{Z}} \sum_{m_2 \in \mathbb{Z}} d[n_1 + m_1 L_{1,j}, n_2 + m_2 L_{2,j}]. \quad (1.5)$$

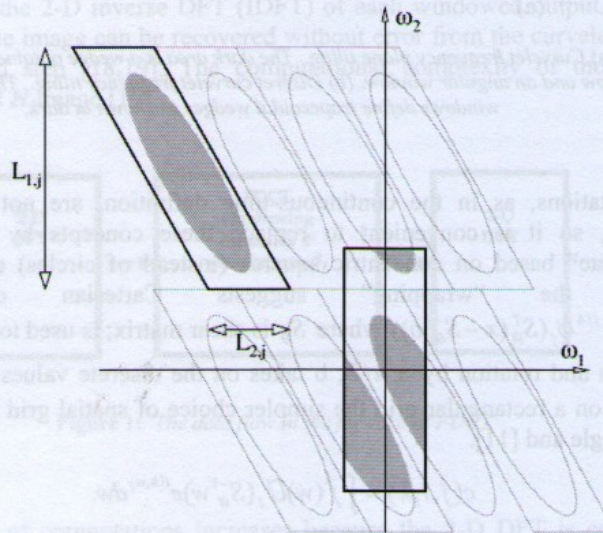


Figure 3: Wrapping data, initially into a rectangle by periodicity. The angle θ is here in the range $(\pi/4, 3\pi/4)$, the black parallelogram is the tile which contains the frequency support of the curvelet whereas the grey parallelograms are the replicas resulting from periodization. The rectangle is centered at the origin. The wrapped ellipse appears "broken into pieces."

The wrapped windowed data, around the origin, is then defined as the restriction of $Wd[n_1, n_2]$ to indices n_1, n_2 inside a rectangle with sides of length $L_{1,j} \times L_{2,j}$ near the origin:

$$0 \leq n_1 \leq L_{1,j}, \quad 0 \leq n_2 \leq L_{2,j}. \quad (1.6)$$

Given the indices (n_1, n_2) originally inside $P_{j,l}$, (possibly much larger than $L_{1,j}, L_{2,j}$), the correspondence between the wrapped and the original indices is one-to-one. Hence, the wrapping transformation is a simple reindexing of the data. It is possible to express the wrapping of the array $d[n_1, n_2]$ around the origin even more simply by using the “modulo” function:

$$Wd[n_1 \bmod L_{1,j}, n_2 \bmod L_{2,j}] = d[n_1, n_2], \quad (1.7)$$

with $(n_1, n_2) \in P_{j,l}$. Intuitively, the modulo operation maps the original (n_1, n_2) into their new position near the origin. For those angles in the range $\in (\pi/4, 3\pi/4)$, the wrapping is similar after exchanging the role of the coordinate axes. This is the situation shown in Figure 3.

Description of the method

In this subsection, we propose a new approach for image denoising that is based on the curvelet transform and removing some of the coefficients heuristically, to obtain a better filtering over the image. We can adjust the parameter of some coefficients over the curvelet transform. Equipped with this definition, the architecture of the FDCT via wrapping is as follows [11]:

1. Apply the 2-D FFT and obtain Fourier samples $\tilde{f}[n_1, n_2], -n/2 \leq n_1, n_2 \leq n/2$.
2. For each scale j and angle l , form the product $U_{j,l}[n_1, n_2] = \tilde{f}[n_1, n_2]$.
3. Wrap this product around the origin and obtain

$$\tilde{f}_{j,l}[n_1, n_2] = W(U_{j,l} \tilde{f})[n_1, n_2], \quad (1.8)$$

where the range for n_1 and n_2 is now $0 \leq n_1 \leq L_{1,j}$ and $0 \leq n_2 \leq L_{2,j}$ (for θ in the range $(-\pi/4, \pi/4)$).

4. Apply the inverse 2-D FFT to each $\tilde{f}_{j,l}$, hence collecting the discrete coefficients $C^D(j, l, k)$. This algorithm has computational complexity $O(N^2 \log N)$.
5. Denoising with the FDCT is carried out in the following way: Once the FDCT is computed, we used a threshold that distinguishes between the less significant coefficients (which represent the noise) and the most significant coefficients consisting of important signal information, and then the less significant coefficients are attenuated. The threshold is selected manually by trial and error.
6. Apply the inverse transform using the IFDCT function for recovering the filtered image.

Experimental results

In this section we present the results processing simulated and experimentally obtained phase-maps. The algorithm was implemented using Matlab 2009 and the toolbox CurveLab 2.1.2 [23].

The first experiment was with a synthetic phase-map (size 200×200), with uniformly distributed noise ranging from 0 to 1. In this case the scales for the FDCT were 5 and angles were 32. The processing time was 2.31 seconds. The Figure 5 shows the obtained results,

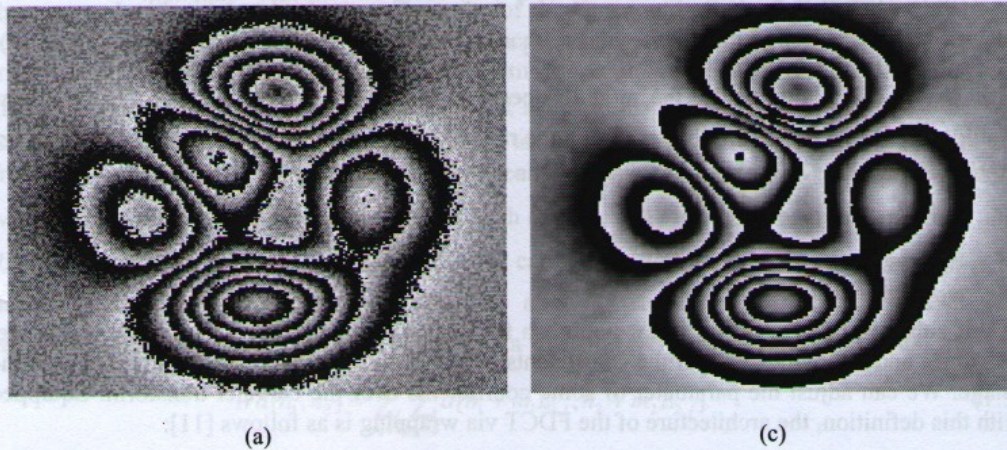


Figure 5: (a) Synthetic noisy phase-map. (c) Denoised phase-map using the FDCT method.

The second experiment was carried out with an experimentally obtained ESPI phase-map (size 480×400), with uniformly distributed noise ranging from 0 to 1. In this case the scales for the FDCT were 4 and 64 angles. The processing time was 3.27 seconds.

Further, we quantitatively evaluate the performance of this method with a comparative parameter, the image fidelity f . The image fidelity f , which is a parameter that quantifies how good image details are preserved after noise removal, is defined as

$$f = 1 - \frac{\sum (I_0 - I)^2}{\sum I_0^2} \quad (1.9)$$

Where I_0 and I are the noiseless images and the estimate image, respectively. A high fidelity value will indicate that the processed image is very similar to the noiseless one. The fidelity for Figure 5 was 0.8840 and the Figure 6 was 0.9465.

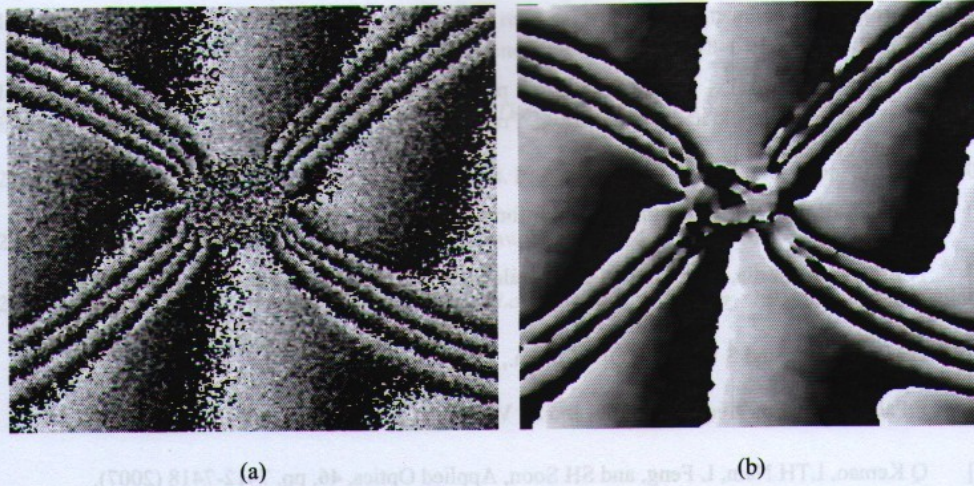


Figure 6: (a) Experimentally obtained ESPI phase-map. (b) Denoised phase-map using the FDCT method.

Conclusion

Denoising phase-map images is an important task for a further processing. Most times phase-map denoising requires the use of special techniques because traditional methods do not always provides satisfactory results. The Curvelet transform has been developed as an alternative to wavelet transform in which frame elements are indexed by scale, location, and orientation parameters. Attenuating less significant coefficients we can properly remove noise. The main advantage of our proposal using the Curvelet transform is that previous estimation of the phase-map orientation is not required, as is the case of recently reported directional filtering techniques. The use of the curvelet transform is a promissory option for interferometric images (Phase-maps and interferograms).

Acknowledgements

We acknowledge the support for the realization of this work to the Consejo Nacional de Ciencia y Tecnología (CONACYT), México, through the project CB-2008-01/102041 and the partial support from the Consejo Zacatecano de Ciencia y Tecnología through the project FOMIX-CONACYT ZAC-2010-C04-149908.

References

- [1] J Buytaert, J Dirckx, Fringe Projection profilometry. Chapter in: Optical methods for solid mechanics: a full-field approach, Rastogi, Pramod, Hack, Erwin-ISBN: 978-3-527-41111-5, Berlin, Wiley-VCH, 2012, pp. 303-344.
- [2] M Gdeisat, and F Lilley, Computer and Information Science, **1**, 1-32 (2007).
- [3] N Escalante, J Villa, I De la Rosa, E González-Ramírez, and M Araiza, SPIE Proceedings, pp. 1 -7 (2011).
- [4] HA Aebischer, and S Waldner, Opt. Comm., **162**, pp. 205-210 (1999).
- [5] F Palacios, E Goncalves, J Ricardo, and JL Valin, Opt. Comm., **238**, pp. 245-251 (2004).
- [6] Q Kemaο, LTH Nam, L Feng, and SH Soon, Applied Optics, **46**, pp. 7412-7418 (2007).
- [7] C Tang, W Wang, H Yan, and X Gu, Applied Optics, **46**, pp. 2907-2913 (2007).
- [8] C Tang, L Han, H Ren, T Gao, Z Wang, and K, Optics Express, **17** (2009).
- [9] J Villa, R Rodríguez-Vera, JA Quiroga, I De la Rosa, E González, Optics and Lasers in Engineering, **46**, pp. 650-656 (2010).
- [10] J Ma and G Plonka, IEEE Signal Processing Magazine, **73**, pp. 1-34 (2004).
- [11] EJ Candès, L Demanet, D Donoho, and L Ying, **5**, pp. 861-899 (2006).
- [12] X Qing, J Guowang, J., Coiling, Z., Zhengde, W., Yu, H. and, Peizhang, Y., Commission VI, WG VI/4, ISPRS.
- [13] Q Kemaο, T Hoai, L Feng, and S Soon, Applied optics, **46**, pp. 7412-7418(2002).
- [14] EJ Candès, F Guo, Signal Processing, **82**, pp. 1519-1543 (2002).
- [15] EJ Candès and DL Donoho, *Curvelets*, [Online] Available: <http://www-stat.stanford.edu/~donoho/Reports/1999/curvelets.pdf>, (1999).
- [16] EJ Candès, and DL Donoho, Saint-Malo Proceedings, ISBN: 978-0-7695-2994-1, pp. 1-10 (2000).
- [17] EJ Candès, DL Donoho, Roy Soc of London Phil Tr A, **357**, pp.2495 (2006).
- [18] J-L Starck, EJ Candès and, DL Donoho, IEEE transactions on image processing, **11**, pp. 670-684 (2002).

- [19] S Palakkal, and KMM Prabhu, "Poisson noise removal from images using the fast discrete curvelet transform", Communications National Conference (NCC), ISBN: 978-1-61284-090-1, 2011.
- [20] S Mallat, *A wavelet tour of signal processing, The Sparse Way*, pp.194-201, (2009).
- [21] P Vandergheynst, and JF Gobbers, IEEE Trans. Image Process., **Vol. 11**, No. 4, pp. 363-372, 2002.
- [22] TM Mitchell, Machine Learning, WCB-McGraw-Hill, first edition, pp. 96-97, 1997.
- [23] E Candés, L Demanet, L Ying, *CurveLab Toolbox, Version 2.0*, [Online] Available: <http://www.curvelet.org/papers/curvelab.pdf>

Abstract

The aim of this work is to present an acoustic-optical (AO) approach to measure the acoustic reflection coefficient of some materials which are not porous and present a flat shape. The method consists of coupling a laser beam with two ultrasonic waves in an AO cell which is filled by distilled water. The first acoustic beam is incident on a flat sample, placed in the bottom of the cell, whereas the second one is reflected by the same sample. This double AO interaction leads to obtain two superposed diffraction patterns. Consequently an interference phenomenon can be observed. Exploiting the interference fringes contrast obtained by the overlapping of the diffraction orders, it was possible to determine the reflection coefficient of three sorts of metal sheets and a plate made of glass, in the frequency range of MHz. All the experimental results are presented and discussed. A practical relation between fringes contrast and the reflection coefficient has been obtained.

Contact information

* ferns.kalyaan@f
 Institute of optics and precision mechanics
 Ferhat Abbas University, Setif, Algeria